LRRK2-mutant microglia trigger dopaminergic neurodegeneration when activated by neuromelanin

Lucas Blasco-Agell[1†], Meritxell Pons-Espinal[1†], Veronica Testa[1†], Gerard Roch[2,3†], Jara Montero-Muñoz[1], Irene Fernandez-Carasa[1], Valentina Baruffi[1], Marta Gonzalez-Sepulveda[2,3], Yvonne Richaud-Patin[4,5], Senda Jimenez[4,5], Thais Cuadros[2,3], Joana M. Cladera-Sastre[2,3], Joan Compte[2,3], Manel Juan-Otero[6], Eduardo Tolosa[6], Angel Raya[4,5,7*], Miquel Vila[2,3,7,8*], A. Consiglio[1,9*]

1. Department of Pathology and Experimental Therapeutics, Bellvitge University Hospital-IDIBELL, 08908 Hospitalet de Llobregat, Spain; Institute of Biomedicine of the University of Barcelona (IBUB), Carrer Baldiri Reixac 15-21, Barcelona 08028, Spain.
2. Neurodegenerative Diseases Research Group, Vall d'Hebron Research Institute (VHIR)-Network Center for Biomedical Research in Neurodegenerative Diseases (CIBERNED), 08035 Barcelona, Spain.
3. Aligning Science Across Parkinson's (ASAP) Collaborative Research Network, Chevy Chase, MD 20815, USA.
4. Regenerative Medicine Program, Bellvitge Biomedical Research Institute (IDIBELL), and Program for Clinical Translation of Regenerative Medicine in Catalonia (P-CMRC), Hospital Duran i Reynals, Hospitalet de Llobregat, 08908 Barcelona, Spain.Centre for Networked Biomedical Research on Bioengineering, Biomaterials and Nanomedicine (CIBER-BBN), 28029 Madrid, Spain.
5. Immunology Department–CDB, Hospital Clinic de Barcelona, Institut d'Investigacions Biomèdiques August Pi i Sunyer (IDIBAPS), University of Barcelona (UB), Barcelona 08036, Spain.
6. Department of Neurology, Hospital Clínic de Barcelona, Institut d'Investigacions Biomèdiques August Pi i Sunyer (IDIBAPS), University of Barcelona (UB), Barcelona, Spain.
7. Catalan Institution for Research and Advanced Studies (ICREA), 08010 Barcelona, Spain
8. Department of Biochemistry and Molecular Biology, Neuroscience Institute, Autonomous University of Barcelona, 08193 Barcelona, Spain
9. Department of Molecular and Translational Medicine, University of Brescia, Brescia, Italy.

[†]These authors contributed equally to this work.

*Correspondence and requests for materials should be addressed to: A.C.(email: consiglio@ub.edu) M.V. (email: miquel.vila@vhir.org) or A.R. (email: araya@idibell.cat)

Abstract

Parkinson's disease (PD) is a progressive and yet incurable neurodegenerative condition characterized by loss of neuromelanin-containing dopamine neurons in the *substantia nigra* of the midbrain. The contribution of non-neuronal cells to neuron degeneration in PD is receiving increasing attention. Here, we generated functional microglia-like cells from induced pluripotent stem cells (iPSC) from patients with PD associated to *LRRK2* mutations, the most common cause of genetic PD, along with their gene-corrected isogenic controls and with iPSC from healthy donors. Microglia-like cells of either genotype did not induce neurodegeneration of healthy dopamine neurons in co-culture experiments. However, LRRK2-mutant microglia became hyperreactive upon LPS stimulation when compared with controls, as judged by cytokine expression profile, production of reactive oxygen species. We then tested α-synuclein and neuromelanin as potential endogenous stimuli for activating mutant microglia. Upon exposure to neuromelanin-containing particles, but not to preformed α-synuclein fibrils, LRRK2-mutant microglia induced the degeneration of healthy dopamine neurons, in a process that could be prevented by pre-treatment with the immunomodulatory drug ivermectin. Finally, the analysis of post-mortem midbrain tissue of LRRK2-PD patients found increased numbers of activated microglia cells in close contact with neuromelanin-containing neurons. Taken together, our findings uncover a potential critical role of neuromelanin-activated microglia in the context of PD progression, and provide an experimental model of PD to test new therapeutic targets.

Keywords: iPSC, Parkinson's disease, microglia, neuromelanin, LRRK2.

Introduction

Parkinson's disease (PD) is an age-associated movement disorder resulting from progressive loss of neuromelanin (NM)-containing dopaminergic neurons (DAn) in the substantia nigra pars compacta (SNpc) and deposition of Lewy bodies (LBs), which mainly consist of α-synuclein[1]. In addition to these two specific hallmarks, glial-related neuroinflammatory responses have emerged as key components of PD physiopathology[2].

While the majority of PD cases are of unknown cause, so called idiopathic PD[3], pathogenic variants in PD-associated genes can be identified in about 15 % of patients[4], with mutations in the *LRRK2* gene accounting for the largest number of patients of familial PD[5].

LRRK2 is a large, ubiquitously expressed protein, containing both GTPase and kinase domains, involved in autophagy-lysosomal pathway, modulation of cytoskeletal dynamics, vesicle trafficking, mitochondrial function and immunity[6]. Notably, LRRK2 expression has been found increased in several peripheral immune cells of PD patients compared to healthy controls[7–10] as well as in microglia after stimulation with lipopolysaccharides (LPS), INF-γ, HIV-Tat protein, manganese, or rotenone[11–14].

Multiple lines of evidence suggest a correlation between mutant LRRK2 and several pathogenic mechanisms linked to PD initiation and progression, including an imbalanced inflammatory signalling[15]. However, little is known about the correlation between LRRK2 mutant microglia activation and PD-endogenous stimuli, such as NM.

NM is a byproduct of dopamine metabolism that progressively accumulates during aging, predominantly in the SN DAn[16,17]. While the functional significance of NM production, if any, remains unknown, it has been hypothesized that NM could play a neuroprotective role by removing excessive cytosolic catecholamine oxidized species, chelating potentially toxic metals or sequestering environmental neurotoxins[18]. Regardless of its putative protective role, recent studies using humanized NM-producing animal models revealed that age-dependent progressive intracellular build-up of NM above a pathogenic threshold ultimately compromised neuronal function and viability, triggering PD-like pathology in both rodents and non-human primates (NHP)[19–21] . Moreover, leakage of NM from dying DAn in the SN from PD brains and NM-producing rodents/NHP triggers an early immune response in the brain, leading to inflammation and oxidative stress[22–26] that could contribute to PD development and progression.

While it has been demonstrated that NM-induced microglia activation can contribute to DAn cell death in primary microglia cultures and in rat models[27,28], no conclusion has been drawn on the impact of LRRK2 mutation on NM-induced microglia activation, and it is still unclear if human derived microglia would respond to NM in the same way of primary one.

To directly investigate the crosstalk between extracellular NM and microglial activation in the context of pathogenic LRRK2 mutation, here we established a humanized co-culture system based on patient-specific iPSC-derived cells. Specifically, we generated iPSC-derived microglia (hMG) from two different PD patients with LRRK2 G2019S mutation (L2-PD) and their respective isogenic controls (L2-PD^{corr}), as well as from healthy individuals (CTL). We then established neuron/microglia co-cultures containing healthy iPSC-derived DAn together with hMG from all conditions. Exposing this system to purified NM extracts allowed us to investigate the potential role of microglia-mediated NM-inflammatory signalling in PD-related neuropathology. Indeed, using this experimental setting, we found that extracellular NM decreases the number of ventral midbrain (vm) DAn in the presence of L2-PD-derived microglia and that this effect is reversed by immunomodulation with FDA-approved drug ivermectin (IVM). The induced neurodegeneration is also specific to NM, given that addition of α-synuclein pre-formed fibrils (PFF) to L2-PD hMG and vmDAn co-culture did not trigger this effect. Overall, our results indicate a deleterious role of NM-activated L2-PD microglia and provide a human-relevant pre-clinical platform for immunomodulatory drug screening in the context of PD.

Results

iPSC-derived hMG express typical microglial markers

We generated human microglia cells (hMG) from iPSC lines following a serum- and feeder-free four-step differentiation protocol[29,30] (**Supplementary Fig. 1a**) from two LRRK2-PD patients carrying the G2019S mutation (L2-PD), one healthy donor (CTL) and two isogenic iPSC line with the LRRK2 G2019S missense mutation corrected (L2-PD^{corr}) (**Supplementary Table 1**). Immunocytochemistry (ICC) detection of key microglia markers showed robust expression of IBA-1, CX3CR1, and TMEM119 in all iPSC-derived hMG after one week in culture (**Fig. 1a-b** and **Supplementary Fig. 1b**). No other cell types, such as astrocytes and neurons, were found as assessed by immunostaining with anti-GFAP or TUJ1 antibody, respectively (**Fig. 1a** and **Supplementary Fig. 1b**). In addition, we found that hMG were positive for the myeloid marker CD11b as well as the scavenger receptor CD163 (**Supplementary Fig. 1c-d**). Microglial identity was further confirmed by quantitative RT-PCR of canonical human microglia-specific genes, including *P2RY12*, *GAS6*, *PROS1*, ME*RTK*, *C1Qa*, and *GPR34*, which were expressed in hMG, but not in iPSCs[31] (**Supplementary Fig. 1e**). Importantly, no differences or evidence of a mutation effect were seen in hMG generation capacity between lines. In addition, when included into ventral midbrain organoids (vmO) to simulate a more physiological environment, hMG adopted a more complex morphology as observed by their ramifications (**Supplementary Fig. 2a-c**).

All together, these results confirm the successful generation of microglia-like cells, which represent a continuous source of human CTL, L2-PD^{corr} and L2-PD microglia for subsequent analyses.

Functional validation of hMG

Next, we aimed at validating hMG using functional and physiological assays. To this end, we first evaluated IL-1β, IFNγ, IL-6 and TNFα cytokine secretion, known to be elevated in PD patients[32–37], from hMG following stimulation by Lipopolysaccharide (LPS) (**Fig. 1c**). As expected, all iPSC-derived hMG robustly responded to LPS with induction of all measured cytokines (**Fig. 1d-f** and **Supplementary Fig. 2d**). However, we found that L2-PD hMG significantly released higher levels of cytokines upon LPS stimulation as compared to CTL or L2-PD^{corr} hMG (**Fig. 1d-f**) and increased the expression of inflammasome-related genes (**Supplementary Fig. 2e-f**).

Given that microglia is involved in synaptic pruning[38–40], we tested the ability of hMG to phagocytize human synaptosomes (SYNs) isolated from human iPSC-derived mature neurons **(Supplementary Fig. 2g-j**). Quantification of pHrodo-flurescent labelled SYNs revealed an efficient engulfment of SYNs by all iPSC-derived hMG lines. However,

we found increased SYNs phagocytosis in L2-PD hMG compared to CTL and L2-PD^{corr} hMG (**Fig. 1g-h**), indicating that the increased L2-PD hMG phagocytic activity depends on LRRK2-G2019S mutation.

L2-PD hMG increases NM uptake and releases ROS

PD neuropathology is characterized by the preferential degeneration of DAn containing NM[23,27] and increased microgliosis[41–43]. To define the interplay between microglia and extracellular NM released from dying neurons in the neurodegenerative process of PD, we first tested the effects of purified NM on microglia activation.

To do that, we exposed hMG to NM extracts purified from a neuronally differentiated SH-SY5Y cell line that produces human-like NM by overexpression of melanin-producing enzyme human tyrosinase[19,44] (**Supplementary Fig. 3a**) and performed time-lapse imaging, qPCR and ROS analyses (**Fig. 2a**). We observed that hMG were highly motile, constantly scanned the microenvironment and extended their filopodia onto NM particles to phagocytose them (**Movie S1**). Sixteen hours after NM exposure, we found that hMG accumulated NM, being the amount of NM particles in L2-PD hMG significantly higher compared to CTL and L2-PD^{corr} hMG (**Fig. 2b-c and Supplementary Fig. 3b**). Moreover, L2-PD hMG moved faster (**Fig. 2d-e and Supplementary Fig. 3c**) and travelled more distance (**Fig. 2f**) than their corresponding controls.

To evaluate whether hMG can be activated by NM, hMG were cultured with and without the presence of NM for 24 h and then harvested to measure gene expression of selected pro-inflammatory and neurotoxic factors. We found that L2-PD hMG increase *IL-1β, IFNγ*, *IL-6, C3* and *TNFα* mRNA expression levels as compared to its isogenic control when exposed to NM (**Fig. 2g-j** and **Supplementary Fig. 3d**). We next assessed hMG activation after NM exposure by measuring dichlorofluorescein (DCF) fluorescence, as indicative of reactive oxygen species (ROS) production. We found that NM increased ROS production in L2-PD hMG as compared to L2-PD^{corr} hMG (**Fig. 2k**).

Taken together, these observations indicate that L2-PD hMG gets activated by engulfed NM and induces the expression of pro-inflammatory cytokines and releases high levels of ROS, raising the possibility of studying their detrimental effects on DAn survival.

L2-PD hMG induces dopaminergic neuronal degeneration upon NM exposure

Next, to study the interaction between ventral midbrain DAn and hMG and the effect of purified NM on DAn survival, we established a 2D neuron/microglia co-culture system. We generated DAn from CTL iPSC[45] and cultured them on top of a human astrocyte feeder layer for 7 days. In a subset of experiments, we used a LV expressing GFP, to visualize the transduced microglia (**Fig. 3a** and **Supplementary Fig. 4a-b)**. In the

absence of NM, we observed highly ramified IBA1-positive hMG in close proximity to DAn stained with Tyrosine hydroxylase (TH) **(Supplementary Fig. 4c-e).** Interestingly, DAn co-cultured with either L2-PD or L2-PD^{corr} hMG appeared well ramified and healthy without any alterations in DAn survival (**Fig. 3b-c)**, thus indicating that L2-PD hMG do not negatively affect TH+ neurons under homeostatic conditions.

We subsequently evaluated the effects of NM-exposed hMG on the survival of CTL iPSC-derived DAn. After eight hours of NM treatment (**Fig. 3a)**, both L2-PD and L2-PD^{corr} hMG suffered a change of morphology towards a more rounded amoeboid shape, indicative of microglia activation (**Supplementary Fig. 4c-e**). Remarkably, only NM-activated L2-PD hMG significantly reduced the percentage of TH+ DAn, compared to a situation without NM (**Fig. 3d-g**). Moreover, surviving DAn displayed a reduced number of branches, indicating an impaired morphology (**Fig. 3d, f** and **Supplementary Fig. 4f-g)**. Similar signs of neurodegeneration were observed when iPSC-derived DAn were treated with NM-exposed L2-PD hMG conditioned medium (MCM) (**Supplementary Fig. 4 h-j)**. These results support a pathogenic effect of NM-activated L2-PD hMG on DAn.

In order to determine whether hMG-induced neuronal degeneration was specific of NM activation, we treated DAn with preformed α-synuclein PFF for eight hours (the time needed to detect DAn degeneration in NM-treated co-cultures), either alone or in the presence of L2-PD hMG (**Supplementary Fig. 5a)**. Whilst NM treated co-cultures triggered TH+ neuronal degeneration already eight hours after exposure, we found that PFF did not induce DAn degeneration even with L2-PD hMG (**Supplementary Fig. 5b-c)**. Altogether, these results suggested that L2-PD hMG induces DAn neurodegeneration under specific PD-associated stimuli such as NM, but not α-synuclein PFF.

Treatment with Ivermectin prevents L2-PD hMG induced dopaminergic neuronal degeneration upon NM exposure

We next investigated whether ivermectin (IVM), an immunomodulatory drug known to switch microglia into an anti-inflammatory phenotype[46,47], could attenuate DAn degeneration induced by NM in our co-culture system. DAn derived from CTL iPSC were co-cultured with L2-PD hMG, exposed to NM and treated with 3μM IVM for 6 hours (**Fig. 3a**). In contrast to untreated conditions, IVM was able to significantly prevent DAn degeneration induced by NM-activated L2-PD hMG (**Fig. 3h-i**). In line with a reduction on L2-PD hMG activation after IVM treatment, we found a significant reduction on the expression of pro-inflammatory cytokines *IL-1β, IL-6, C3* and *TNFα* in L2-PD hMG monocultures (**Fig. 3j-m**).

Overall, our findings support the concept that microglia activated by extracellular NM may directly contribute to PD neurodegeneration and that immunomodulatory interventions at early disease stages could provide therapeutic benefit.

Microglial activation is increased in post-mortem brains from L2-PD patients

To determine whether the results obtained *in vitro* using hMG lines could be relevant to humans, we next assessed microglia activation in the SN of post-mortem brains from L2-PD patients, compared to age-matched controls (**Supplementary Table 2**). The total number of IBA-1-positive microglial cells was significantly higher in L2-PD brains compared to control subjects (**Fig. 4a**). More importantly, a higher number of these microglial cells exhibited an amoeboid morphology in L2-PD cases, indicative of its activation, compared to non-PD controls (**Fig. 4b-c**). In contrast, the number of non-reactive (ramified) microglia did not differ between L2-PD and control brains (**Fig. 4b-c**). In L2-PD cases, activated microglia was usually found engulfing NM granules (**Fig. 4c**). These results are compatible with the *in vitro* findings in NM-exposed hMG and reinforce the concept that NM-linked microglial activation may contribute to PD pathogenesis.

Discussion

Neglected for decades, inflammation has gained attention in the latest years as a possible modulatory approach for PD[2,48–50]. Being microglia the main immunocompetent cell in the CNS, researchers have focused on these cells to understand how inflammation could impact the pathophysiology of PD. Among other stressors, NM has been proven to induce MG activation and trigger neuronal cell death[19–21,23–25,27,28,51,52]. However, due to methodological limitations and the restricted availability of human samples, MG biology and NM impact on its activation in PD has only been partially studied using non-human models[19–21,27,28]. This limitation was bypassed thanks to the advent of iPSC technology, offering unlimited possibilities to substitute traditional methods and to generate human-derived microglia-like cells with a wide variety of protocols. Taking advantage of this technique, we were able to show here for the first time the impact of NM-induced activation on a human-derived, LRRK2 mutated microglia, and how this impact ultimately affects DAn death.

To be able to pinpoint specifically the effect of the LRRK2 mutation in MG upon activation with NM, we generated hMG from 1 Control, 2 LRRK2-PD and 2 corrected Isogenic-PD iPSC lines. All iPSC-derived hMG expressed several key microglial markers, confirming they are *bona fide* microglia[53]. At basal level, all generated hMG were able to phagocyte particles, showed high motility, became activated and released cytokines when exposed to different stimuli. Of interest, we found L2-PD hMG to be highly motile and phagocytic if compared to its isogenic counterpart, a point that has been previously debated[11,15,54–56]. We also confirmed that L2-PD hMG had an exaggerated inflammatory response upon stimulation with LPS[12,15,57,58].

The novelty of the current study relies on the description of how human-derived, LRRK2 mutated MG respond to NM stimulus. Although previous reports indicated that NM can induce MG activation in post-mortem brains[59–62] and experimental animal models[19–21,23–25,27,28,51,52], our results show for the first time that NM can be actively phagocyted by human MG, activating ROS and cytokine production. Importantly, both L2-PD hMG lines presented increased phagocytosis of NM particles with subsequent increase of ROS and cytokine production as compared to L2-PD^{corr} hMG, confirming that this over-active phenotype can be directly attributed to the LRRK2-G2019S mutation.

Using then a DAn-MG co-culture platform we were able to uncover that NM, but not α-synuclein PFF, induces neurodegeneration in TH+ neurons only when L2-PD hMG is present. This is at least partially due to the fact that L2-PD hMG enhance, upon NM stimulation, the production of pro-inflammatory cytokines. In accordance to this,

treatment of the co-culture with the immunomodulatory drug ivermectin, which rescued the increased cytokine levels induced by NM in L2-PD hMG, was able to prevent the NM-induced neurodegeneration. The fact that α-synuclein PFF did not trigger the same neurodegenerative effect as NM may be due to the activation of a different downstream cascade, or to a different cellular internalization pathway. This finding is also in line with previous *in vivo* data using a rodent model producing human-like NM, that stated that progressive NM accumulation with age leads to an early inflammatory response linked to neuronal dysfunction/degeneration[19,23]. Interestingly, the results obtained from post-mortem human brains, where the LRRK2-PD group displays increased microgliosis and microglial activation, further support this concept.
Although a deep understanding of the downstream cascade mechanisms underlying the pathogenic effects of NM-induced inflammation has still to be defined, our results suggest that a possible therapeutic option for PD patients could be focused on modulating inflammatory response in the degenerating SNpc to halt or delay the progression of the disease.

While our model allows for a robust evaluation of the LRRK2 mutation contribution to human MG activation upon NM stimulation, several limitations should be considered. Firstly, the *in vitro* set-up is limited in terms of complexity that can be reached and is characterised by high variability. To partially overcome these issues, all experiments were performed at least in triplicates and evaluating two independent patient-derived lines and their respective isogenic controls. Moreover, while the presence of astrocytes as feeder layer in the DAn-hMG co-culture allowed us to have a more stable platform, where neurons were viable enough to test the effect of both NM and IVM, it may also partially mask the degenerative phenotype induced by NM.

Overall, our results indicate that L2-PD mutant microglia is not pathogenic *per se* but can become deleterious when overstimulated specifically by NM released from dying neurons. These results may have important therapeutic implications for future intervention at early disease stages, in which small amounts of extracellular NM are sufficient to trigger a major inflammatory response before overt neurodegeneration[52]. Moreover, the system established could serve as a platform to test new therapeutical targets.

Experimental procedures

iPSC derived microglia (hMG)

In order to generate hMG cells from iPSCs, we have followed an already published serum- and feeder-free four-step protocol described by Douvaras et al.[29] built on previous studies from Yanagimachi et al.[63] and adapted by Mesci et al.[30]. A summary of the iPSC used is described in Table 1. Unless specified, all growth factors, small molecules and cytokines employed during this project were purchased from PeproTech®. Single iPSC colonies were manually passaged onto fresh Matrigel-coated 6 cm^2 plastic plate. After 2-4 days, protocol started by supplementing mTeSR™1 medium with 80 ng/mL of Bone Morphogenetic Protein (BMP)-4 every day from day 0 to day 4. From day 5, SP34 medium was employed, which consisted of StemProTM-34 SFM (Gibco™) with 1% of P/S and 1% of Ultraglutamine (Glut; Lonza). For two days, SP34 medium was supplemented with 80 ng/ml of VEGF, 100 ng/ml of Stem Cell Factor (SCF) and 25 ng/ml of Fibroblast Growth Factor (FGF)-2. After day 7 until day 14, SP34 was supplemented with 50 ng/ml of Fms-like tyrosine kinase 3-Ligand (Flt3-L), 50 ng/ml of IL-3, 50 ng/ml of SCF, 5 ng/ml of Trombopoietin (TPO) and 50 ng/ml of M-CSF, changing the medium at day 10. The last step consisted on the addition to SP34 of Flt3-L, M-CSF and 25 ng/ml of GM-CSF from day 14, changing the medium every 3-4 days. At day 35, floating hMG progenitors were collected from the culture's supernatant and passed through a 70 µm Filcon™ Syringe-Type nylon mesh (BD Biosciences) to ensure a single-cell suspension and to remove cell clumps. Cells were counted, centrifuged at 300x*g* for 10 minutes and cultured in Roswell Park Memorial Institute (RPMI) 1640 Medium (Gibco™) with 1% of P/S and 1% of Glut, supplemented by M-CSF and 50 ng/ml IL-34. Medium was changed with fresh factors every 2-3 days. hMG progenitors were plated onto Matrigel-coated glass coverslips in 24-well plates (25,000 cells/well), on uncoated 96-well plates (10,000 cells/well) or 6-well plates (200,000 cells/well) depending on the experiment. hMG mature cells were cultured for one week, before being used for experiments. For treatments, 100 ng/mL of LPS or 5 ug/mL of NM were added for a total of 24 hours.

iPSC-derived vmDAn

Generation of vmDAn from iPSCs was performed following the floor plate (FP) derivation protocol[64,65]. iPSC medium was changed to Serum Replacement Medium (SRM), which was based on KO-DMEM with 15% of KO Serum Replacement (KO-SR; Gibco™), 1 % of P/S, 1% of Glut, 1% of Non-Essential Amino Acids (NEAA; Lonza), and 10 µM of β-Mercaptoethanol (BME; Gibco™). The first day, SRM was supplemented with 100 nM of LDN193189 hydrochloride (LDN; Sigma-Aldrich) and 10 µM of SB 431542 (SB; Tocris

Bioscience). From there and during all the differentiation, cells were maintained under hypoxic conditions (37 ºC Temperature, 5% CO_2 and 5% O_2). From day 1 to day 5, SRM medium was supplemented with same concentrations of LDN and SB and adding 1 µM of Smoothened Agonist (SAG; Merck Millipore), 2 µM of Purmorphamine (Tocris Bioscience), and 100 ng/mL of FGF-8. From day 3 onwards, 3 µM of StemMACS™ CHIR99021 (CHIR; Miltenyi Biotec) were also added. From day 5, medium was progressively switched from SRM to N2, which consisted of Neurobasal™ Medium (Gibco™), 1x N2 supplement (Gibco™), 1% of P/S and 1% of Glut. On day 11, medium was changed with N2 supplemented with LDN and CHIR and cells could be either expanded as FP progenitors or matured to vmDAn. The additional step to expand, freeze and thaw FP progenitors was adapted from Fedele et al.[65]. Cells were maintained in N2 supplemented with LDN and CHIR at day 11, until reaching 90% of confluency within the plate. To differentiate FP progenitors into vmDAn, medium was changed to B27-vitA, which contained Neurobasal™, 2x B27™- vitamin A (Gibco™), 1% of P/S and 1% of Glut. Every two days, medium was fully changed with B27 supplemented with 20 ng/mL of BDNF, 20 ng/mL of Glial cell-line Derived Neurotrophic Factor (GDNF), 1 ng/mL of TGF-β3, 10 µM of Deoxyadenosine Triphosphate (dAPT; Calbiochem), 0.5 mM of Dibutyryl cyclic-Adenosine Monophosphate sodium salt (cAMP; Sigma-Aldrich) and 0.2 mM of L-Ascorbic Acid (AA; Sigma-Aldrich). On day 20, cells detached with Accutase (Merck Millipore), counted and centrifuged at 300x*g* for 5 minutes. Cells were plated on 6-well or glass coverslips in 24-well plastic plates with a triple-coating of 15 µg/mL Poly-L-Ornithine solution (Sigma-Aldrich), 3 µg/mL of Laminin (Sigma-Aldrich) and 2 µg/mL of Fibronectin (Sigma-Aldrich) to a density of 100,000 cells/cm^2. From day 20 onwards, half of B27 with factors was changed every 3-4 days until vmDAn were used for experiments.

iPSC-derived organoid generation

Ventral midbrain organoids (vmO) were generated from iPSC using a protocol adapted from Kriks et al.[64]. Unless specified, concentration of molecules and cytokines remained as the previous vmDAn protocol. Briefly, iPSCs were grown until 90% of confluence and 10 µM of RI was added to culture plate 4/6 hours before starting the protocol. Then, cells were dissociated in 1:1 accutase/DPBS, detached and centrifuged at 800x*rpm* for 5 minutes. Cell pellet was resuspended in 1 mL of fresh mTeSR™1, passed through a 40 µm cell strainer (Clear Line®) and counted. Dissociated iPSCs were plated in ultra-low attachment 6-well plastic plate (Corning®) at a density of 4 x 10^6 cells per well, with mTeSR™1 medium supplemented with 10 µM of RI. From then on, cells were kept under

rotation on CO2 resistant orbital shaker (Leica) at 120*xrpm* and maintained under normal incubation conditions.

After 2 days, medium was replaced with SRM supplemented with LDN and SB, a dual SMAD inhibition to promote neuronal commitment[66]. On day 4, and every 3 days, half of SRM medium was replaced with fresh factors and the addition of SAG, Purmorphamine, CHIR and AA. On day 12, SRM medium was replaced by NBN2B27-vitA, which consisted of Neurobasal™ supplemented with 1x N2, 2x B27™-vitA, 1% of P/S and 1% of Glut. N2B27-vitA was changed every other day by the addition of 100 nM of LDN, 1 µM of SAG, 2 µM of Purmorphamine, CHIR and AA, 50 ng/mL of FGF-2, and 50 ng/mL of Endothelial Growth Factor (EGF; R&D Systems), to promote conversion towards a DAn fate (Kriks et al., 2011). From day 22 onwards, spheres were matured to vmO in B27-vitA supplemented with BDNF, GDNF, TGF-β3, cAMP and AA. Half of the medium was changed every 2-3 days and vmO were cultured until day 45, before being used for experiments.

2D and 3D Neuron/Microglia co-culture systems

In order to visualize iPSCs-derived hMG within 2D/3D co-cultures, iPSCs were transduced with a lentiviral vector (LV) expressing Green Fluorescence Protein (GFP) under the Phosphoglycerate Kinase (PGK) ubiquitous promoter as previously described[67]. Briefly, iPSCs were detached and 10^6 iPSCs were infected in 100 uL of mTeSR™ within a 15 mL Falcon tube with a mean of infection (MOI) of 10. Cells were incubated under normal conditions for 1 hour and plated in a 6 wp with 1 mL of mTeSR ON. After 16-18 hours, 1 mL of mTeSR™ was added. Fluorescence was checked after 72 hours under an inverted microscope.

To study neuron/microglia interactions, we generated 2D co-culture system with iPSC-derived vmDAn. First, mature GFP-iPSC-derived hMG were conditioned with medium from vmDAn without B27-vitA, since it contains several products that could compromise microglial functioning[68]. One-week later, hMG were detached with accutase, counted and plated on top of day 42 vmDAn on a human astrocyte feeder layer, at a ratio of 1 hMG per every 2 neurons. Astrocytes feeder layer was employed for every analysis where we needed to assess neuronal health. Co-culture medium consisted of RPMI with Neurobasal™ 50/50% supplemented with 1% Glut, 1% P/S, M-CSF, IL-34, BDNF, GDNF, TGF-β3, cAMP and AA. Half of the medium was changed every 2-3 days. vmDAn and hMG were co-cultured for 1 week in hypoxia conditions, before being used for experiments. For culture treatments, 0.5 ug/mL of NM was added to co-cultures for 8 hours, and after 2 hours IVM 3 uM was added, for a total of 6 hours. In case of PFF, 10 ug/mL were added for 8 hours. Images were taken under a 63x objective employing a

confocal microscopy. vmDAn morphology and neurite complexity were assessed by ICC staining of TH and analyzed by Sholl analysis[69] using the Simple Neurite Tracer plugin from ImageJ. hMG morphology was analyzed for circularity employing ImageJ. Reconstruction of vmDAn and hMG were performed with IMARIS. Surface of vmDAn was generated with a Smooth of 0.103 µm and a Background subtraction of 5 µm. Surface of hMG was generated with a Smooth of 0.103 µm and a Background subtraction of 3 µm. For the 3D co-culture system, one vmO was manually placed in a well of a U 96-wp with 50.000 GFP-hMG and incubated under normal conditions in an orbital shaker for 24 hours. Then, every organoid was collected and plated on low-adhesion 6-wp. Co-culture medium was replaced every 2-3 days. vmO and hMG were co-cultured for 1 week in normal incubation conditions in agitation, before being used for experiments. 100 ng/mL of LPS (Sigma-Aldrich) was added for 72 hours to co-cultures to study hMG morphological changes. Reconstruction of hMG was done with IMARIS as explained in *4.6.2.* Volume, sphericity, and Object-Oriented Bounding Box Length C were taken as parameters for hMG morphology.

Immunocytochemistry

Cells plated in 24-well plates were fixed before any ICC staining using 4% of Paraformaldehyde (PFA; EMS) at RT for 15 minutes. Excess of PFA was removed from the culture wells with three washes of 15 minutes with DPBS. For whole vmO IN TOTO ICC, samples were fixed in PFA at 4ºC for 2 hours and rinsed 3 times with TBS for 20 minutes. For ICC of cryosectioned vmO, samples were fixed in 4% PFA at 4ºC Overnight (ON). Fixed vmO were transferred to 30% Sucrose (Sigma-Aldrich) solution at 4ºC ON. vmO were placed on plastic molds with O.C.T.™ compound (Tissue-Tek®) at -80ºC until processing. Cryopreserved vmO were sectioned (20 µm thick) on a cryostat (Leica) and mounted in Menzel-Gläser Superfrost® PLUS coverslips (Thermo Fisher Scientific), dryed at RT ON and stored at -20º C for further ICC staining.

To stain hMG, we used a low Triton X-100 (Triton; Sigma-Aldrich) protocol. Coverslips were placed on Menzel-Gläser Superfrost® Microscope slides (Thermo Fisher Scientific) inside a humid chamber. Samples were then rinsed in 1X Tris-Buffered Saline (TBS) before being blocked at RT for 2 hours with Blocking Solution (BS), which consisted of TBS with 0.01% of Triton and 3% of Donkey Serum (DS). After that, samples were incubated with primary antibodies at 4ºC for 48 hours (see **Supplementary Table 1**). Samples were rinsed and blocked again with BS at RT for 1 hour and incubated with secondary antibodies for 2 hours at RT protected from light. All secondary antibodies employed were from Alexa Fluor Series (Jackson ImmunoResearch Europe) at a concentration of 1:250. After that, samples were rinsed TBS and nuclei were

counterstained with 0.5 µg/mL of 4',6-Diamidino-2-phenylindole (DAPI; Abcam) at RT for 10 minutes. Samples were mounted within a glass coverslip (Corning®) with Polyvinyl Alcohol-1,4-Diazabicyclo-Octane (PVA-DABCO; Sigma-Aldrich). Mounted slides were dried at RT for 30 minutes protected from light and stored at 4ºC before analysis. To stain vmDAn, 2D co-cultures or vmO cryosections, we used a high Triton protocol. In this way, the protocol timing and procedures were the same as explained, except that rinses were done with TBS with 0.1% of Triton and BS consisted of TBS with 0.3% of Triton and 3% of DS.

For the whole organoid structures, *IN TOTO* ICC staining was performed. vmO were rinsed with TBS and incubated with an antigen retrieval buffer composed by Sodium Citrate Tribasic (Sigma-Aldrich) with a pH of 9 at 60ºC for 1 hour. vmO were rinsed in TBS at RT in agitation (Labnet International) and permeabilized with TBS plus 0.5% Triton and 6% DS at 4ºC ON in agitation. Samples were then incubated with primary antibodies (see **Supplementary Table 1**), diluted in BS (TBS with 0.1% Triton and 6% DS) at RT at 4ºC over-the-weekend in agitation. After 3 days, samples were rinsed with BS at RT and incubated with secondary antibodies (diluted in BS) at 4ºC ON in agitation. The day after, vmO were rinsed TBS and nuclei were counterstained with 2.5 µg/mL DAPI (diluted in TBS). Samples were mounted with PVA-DABCO in a glass coverslip, dried and stored at 4ºC for further imaging.
Images were acquired using Zeiss AXIOIMAGER Z1 with an ApoTome (Zeiss Microscopy) microscope using a Cascade CCD camera (Photometrics). For confocal images, Zeiss AXIOIMAGER Z1 with an SPE confocal system or a Zeiss LSM 880 were employed (Zeiss Microscopy). Image acquisition was realized with ZEN pro software (Zeiss Microscopy) and subsequently analyses were performed using ImageJ (NIH), Photoshop® (Adobe) and IMARIS (Bitplane copyright).

Flow Cytometry

Cells were detached, centrifuged at 300x*g* for 10 minutes and pellet was incubated with 1:50 conjugated antibody in MACS buffer for 15 minutes protected from the light (see **Supplementary Table 2**). After that, cold MACS buffer was added, and cells were centrifuged at 300x*g* for 10 minutes. Cell pellet was resuspended in cold MACS buffer and incubated with 1:500 of Propidium iodide (Pi) at RT for 5 minutes to determine cellular viability of the culture. Unstained cells were used as negative controls. FC measurement was done with the Gallios cytometer (Beckman Coulter Life Sciences) with the specific filters for each fluorochrome. Analyzes of staining percentage and

fluorescence intensities were done with Kaluza software (Beckman Coulter Life Sciences).

Gene expression analysis

RNA was extracted using a RNeasy® Mini kit (Qiagen) according to manufacturer's instructions and quantified with a NanoDrop one spectrophotometer (Thermo Fisher Scientific). Reverse transcription into complementary cDNA was performed with the Superscript III First-Strand Synthesis System (Invitrogen™) to a final concentration of 2 ng/µL. Gene expression was measured by real time quantitative Reverse Transcription Polymerase Chain Reaction (qRT-PCR). 8 ng of cDNA were loaded in every well of a MicroAmp™ Optical 384-well Reaction Plate (Applied Biosystems™) with 10 nM of forward and reverse primers (Life Technologies; see **Supplementary Table 3**) and PowerUp™ SYBR™ Green Master Mix (Applied Biosystems™). Plate was run in a 7900HT Fast Real-Time PCR System with 384-well Block Module (Applied Biosystems™) following a standard cycling mode. Cycling values were normalized to the housekeeping gene β-Actin and the relative fold gene expression of samples was calculated using the $2^{-\Delta\Delta Ct}$ method.

Cytokine Array

The EMD MILLIPLEX® MAP Human Cytokine/Chemokine/Growth Factor Pane A – Immunology Multiplex Assay (Merck Millipore) was employed to simultaneously analyze TNF-α, IL-1β, IL-6, and INFγ with Bead-Based Multiplex Assay using the Luminex® technology. Culture supernatants from non-stimulated and 24-hour LPS-stimulated hMG were collected and stored at -80 ºC for long storage. Unless specified. Quality Controls (QC) and Human Cytokine Standard (STD) were prepared with deionized water by serial dilutions as manufacturer's instructions. Assay Buffer was used for Background or STD 0. Briefly, wells were filled with 200 µL of Wash Buffer (WB), sealed and mixed at RT for 10 minutes on a Thermomixer Comfort plate shaker (Eppendorf™) at 500-800 rpm. Plate was firmly tap upside down on absorbent paper and 25 µL of each STD and QC with 25 µL of RPMI medium in duplicates. 25 µL of sample with 25 µL of Assay Buffer were added in duplicates. Finally, 25 µL of the mixed antibody-bead preparation was added to every well and incubated at 2-8ºC ON in a plate shaker.

The day after, well contents were gently removed by firmly attaching plate to a handheld magnet and washed with WB for 3 times. Then, 25 µL of Detection Antibodies were added into each well and incubated at RT for 1 hour on a plate shaker. After that, 25 µL of Streptavidin-Phycoerythrin were added into each well and incubated at RT for 30 minutes on a plate shaker. Well contents were gently removed with a handheld magnet and washed with WB for 3 times. Antibody-beads were resuspended by adding 150 µL

of Sheath Fluid to all wells and incubated at RT for 5 minutes on a plate shaker. Finally, plate was run on a multiplex system Luminex® 200™ (Invitrogen™). Probe heights of every antibody were adjusted according to Luminex® recommended protocols employing the xPONENT® software (Luminex®). Mean Fluorescent Intensity of every analyte was analyzed using a 5-parameter logistic or spline curve-fitting method for calculating analyte concentrations in samples.

Synaptosome extraction

Mature iPSC-derived cortical neurons were obtained from neural progenitor cells (NPCs) as described[66,70]. Synaptosomes (SYNs) were then extracted from mature iPSC-derived cortical neurons using Syn-PER™ Synaptic Protein Extraction Reagent (Thermo Fisher Scientific). 1x of protease inhibitors (Roche) were added to the Syn-PER™ Reagent immediately before use. 200 µL of Syn-PER™ Reagent was added to each 6-wp well and cells were lifted from the surface using a cell scraper (Biologix). Samples were centrifuged at 1200x*g* for 10 minutes at 4ºC. Supernatant was transferred to a new tube and centrifuged at 15000x*g* for 20 minutes at 4ºC. Pellet containing SYNs was resuspended in Syn-PER™ Reagent. SYNs concentration measured using the Bradford assay solution (Bio-Rad Laboratories) and protein concentration was quantified by optical density in a PowerWave™ XS multiplate reader (Biotek®). Resulting SYNs were frozen in 5% (v/v) Dimethyl sulfoxide (DMSO) at -80 ºC for extended periods, until pHRodo™ Red (ThermoFisher Scientific) conjugation.

Western Blot

For protein isolation, cell pellets were resuspended in RIPA buffer with 1X protease inhibitors, sonicated, and centrifuged at 10,400x*g* for 10 minutes at 4°C. Supernatant was collected and protein concentration was determined by Bradford assay. Protein was mixed with 6x LSB (Sigma-Aldrich) and 4% DTT (Sigma-Aldrich) and heated at 95 ºC for 5 minutes in a Thermomixer. Samples were subjected to SDS-PAGE on 8 to 12% of polyacrylamide and samples were run with a PowerPac Basic (Bio-Rad Laboratories) at 90-120 Volts for 60-90 minutes in a Mini-Protean® 3 Cell (Bio-Rad Laboratories). Gel was transferred at 350 Amperes for 120 minutes onto pre-activated polyvinylidene difluoride (PVDF) or Nitrocellulose membranes in a Mini-Protean® 3 Cell (BioRad Laboratories). Correct protein transfer was checked by red Ponceau S Solution (Panreac). Membrane was rinsed 3 times with TBS with 0.1% of Tween20 and blocked at RT for 1 hour with 5% milk or 5% BSA and incubated with primary antibody at 4°C ON (see **Supplementary Table 4**). The day after, membrane was rinsed and incubated with secondary Horseradish Peroxidase (HRP)-labelled antibody at RT for 1 hour. After

rinsing, signal was developed with ECL™ start Western Blotting Detection Reagent (GE Healthcare Amersham™) and images were obtained using a ChemiDoc System (Bio-Rad Laboratories). Protein amount was expressed as a ratio between the band intensity of the protein of interest and the loading control protein β-Actin or Glyceraldehyde-3-Phosphate Dehydrogenase (GAPDH).

pHrodo labeled synaptosome phagocytic assay

Appropriate amount of SYNs were thawed and centrifuged at full speed for 3-4 minutes at 4 ºC. Pellet was resuspended and well-mixed in cold 100 mM of sodium bicarbonate, pH 8.5 to a concentration of 1 mg/mL. SYNs were then incubated with amine-reactive pHrodo Red Succinimidyl Ester (SE) dye (Thermo Scientific) for 60 minutes at RT in a twist shaker (Labnet International). Conjugated SYNs were rinsed with DPBS and centrifuged at full speed for 7 times[71]. 10 µg/mL of SYNs were added to hMG plated on a CellCarrier™-96 Ultra Microplate (Perkin Elmer®) and imaged using 20x objective of a Zeiss SP05 confocal microscopy, maintaining constant levels of temperature (37ºC) and CO_2 (5%). Four to five images were taken every minute for 5 hours using the phase-contrast and red fluorescence mode. 6 hours LPS pre-stimulated cells were employed as positive phagocytic controls. Phagocytic Index (PI) was quantified using ImageJ, extracting background from the red fluorescent pHrodo. Total fluorescence per image was divided by the total number of cells per image[72]. PI values for every hour of the time lapse were plot and the area under the curve (AUC) was quantified to perform statistical analysis.

Isolation of pure NM extracts from cultured TR5TY6 neuroblastoma cells

A stable inducible SH-SY5Y cell line expressing human tyrosinase (TR5TY6) under the transcriptional control of the T-Rex TM Tet-On system (Invitrogen) was provided by Dr. T. Hasegawa (Department of Neurology, Tohoku University, Sendai, Japan[19]. Cells were confirmed negative for mycoplasma contamination by routine PCR analysis. Cells were maintained in low-glucose (1 g/L) Dulbecco's modified Eagle's (Gibco) medium with penicillin/streptomycin and the appropriate selection of antibiotics (7 µg/mL blasticidin and 300 µg/mL Zeocin, both from Life Technologies). A summary of the cell culture and isolation protocol can be seen in **Supplementary Figure 3**. Briefly, TR5TY6 cells were seeded for NM isolation at 3×10^6 cells/plate onto 15-cm plates. At 24 h after seeding, cells were differentiated with 10 µM retinoic acid (RA; Sigma-Aldrich) for 3 days, followed by 80 nM 12-O-tetradecanoylphorbol-13-acetate (TPA; Sigma-Aldrich) for 3 extra days prior to hTyr induction with 2 µg/mL doxycycline (Sigma-Aldrich) for 6 days. Cells were harvested with medium using a cell scraper, centrifuged for 5 min at 300g at 4 °C, and

washed three times with phosphate buffer saline (PBS). Cell pellets were stored at −80 °C until the day of analysis.

NM isolation was performed as previously described, with some modifications[73]. Briefly, each 2 cell pellets (typically of 2 x 10^7 cells each) were thawed at RT and washed in 10 ml of 0.05 N phosphate buffer pH 7.2 and centrifuged at 10,000 x g for 15 min at RT. This washing and centrifugation step was repeated prior the sonication of the resulting pellets in 10 ml of 5 mg/ml SDS in 75 mM Tris pH 7.5 until total resuspension. After a 3 h incubation at 37ºC in a shaking water bath, samples were centrifuged at 10,000 x g for 30 min at RT. Pellets were then incubated for 3 h at 37ºC with 2ml of 5 mg/ml SDS in 75 mM Tris pH 7.5 with 0.33 mg/ml proteinase K (Qiagen). At this point, samples were transferred to microtubes, pooled and subjected to a series of washing steps followed by centrifugations (10,000 x g for 30 min at RT) including: 1 ml of 0.9% NaCl (Sigma-Aldrich), 1 ml of water, 1ml of methanol (Sigma-Aldrich), 1 ml of hexane (Sigma-Aldrich). A 25 µl aliquot was taken from the water solution to quantify NM concentration. After the last centrifugation of hexane-diluted samples, supernatants were discarded and pellets were allowed to dry in a fumehood, fast-freezed by liquid nitrogen immersion and stored at -80ºC. NM concentration of samples was quantified by measuring its absorbance at 405 nm with a NanoPhotomer NP80 (Implen). The calibration curve was prepared by serially diluting a stock solution of 1 mg/ml in 1 M NaOH synthetic melanin to cover the range of 1000 to 15 µg/ml. Pure NM extracts were sonicated in a UCI Ultrasonic cleaning bath sonicator for 15 minutes and stored at -80 ºC until use. For NM experiments, a 5ug/ml concentration in mono-cultures and an 0.5 ug/mL in co-cultures was used.

Neuromelanin phagocytosis assay

For NM phagocytosis uptake analysis, we performed a time lapse imaging video. One-week hMG were plated in plastic 12-wp and placed on a Zeiss AXIOIMAGER Z1 maintaining constant levels of temperature (37 ºC) and CO_2 (5%). 5 ng/mL of NM were added to cultures and 2 images were taken from every well in duplicate every 2 minutes for 16 hours, using the phase-contrast mode. Cells were tracked and particles of uptaked NM were counted for every hour. Cells that died or moved out of the frame were excluded from the analysis. Accumulated NM was plotted during time and AUC was quantified to perform statistical analysis. After 24 hours in culture with NM, cell pellets and supernatants of non-stimulated and NM-stimulated cultures were collected and stored at -80 ºC for further analyses.

Motility analysis

Motility of hMG was assessed in 16 hours-time lapse experiments and analyzed using the Manual Tracker plug of ImageJ. Analyses were done with Chemotaxis and Migration Tool free software version 2.0 (Ibidi®). Velocity (µm/minute) and accumulated distance were evaluated. Accumulated distance refers to the path made by the cell from the starting point to the endpoint.

Intracellular ROS measurement

Intracellular ROS was measured in hMG exposed to 5 ng/mL NM for 24 hours using 2′,7′-Dichlorodihydrofluorescein diacetate ($DCFH_2$-DA) probe (Sigma-Aldrich), which turns highly fluorescent upon oxidation. Ten minutes before adding the probe, hydrogen peroxide (1:25) was added to a well as a positive control of oxidation and absolute ethanol as negative control. Then, 500 µM of $DCFH_2$-DA were added for one hour at 37ºC. After that, cells were rinsed and recovered with a scrapper in PBS with 1% Triton. Samples were placed in CellCarrier™-96 Ultra Microplate and fluorescence was measured within a FLUOstar Omega microplate reader (BMG LABTECH) at 485nm/530nm. Results were normalized to protein concentration measured using a Micro BCA™ Protein Assay Kit (Thermo Fisher Scientific).

Human post-mortem brain tissue

Paraffin-embedded midbrain sections (5 µm) from PD patients with LRRK2 G2019S mutation (L2-PD; n = 6) and age-matched control individuals (n = 32) were provided by the Neurological Tissue BioBank at IDIBAPS-Hospital Clinic (Barcelona, Spain). Detailed information about these subjects is provided in Table 2. Informed written consent was obtained from all human subjects. All procedures were conducted in accordance with guidelines established by the BPC (CPMP/ICH/135/95) and the Spanish regulation (223/2004) and approved by the Vall d'Hebron Research Institute (VHIR) Ethical Clinical Investigation Committee [PR(AG)370/2014]. Samples were deparaffinized at 63 ºC for 30 minutes and quenched in xylene 2 times for 10 minutes at RT. To hydrate the tissue, samples were sequentially transferred to a 100% ethanol solution for 10 minutes, a 95% ethanol solution for 10 minutes and a 70% ethanol solution for 5 minutes. Samples were then rinsed for 5 minutes 3 times in 1X Tris-Buffered Saline (TBS) and the endogenous peroxidase blocked for 15 mins using a 1X TBS solution with 3% H_2O_2 and 10% (vol/vol) methanol. Samples were rinsed again for 5 minutes 3 times in 1X TBS. Epitope unmasking for 20 minutes with 10 mM citrate buffer pH6 at 95 ºC was followed by cooling for 20 minutes at RT. Samples were rinsed for 5 minutes 3 times with 1X TBS – Triton

0.5% buffer. Samples were then blocked for 1 hour using 1X TBS with 5% normal goat serum (NGS; Palex). Samples were subsequently incubated with anti-IBA1 primary antibody (host: rabbit; reactivity: human; concentration: 1:500; source: Abcam; reference: #ab178846) in 1X TBS with 2% NGS ON at 4 °C. Samples were rinsed for 5 minutes 3 times with 1X TBS before incubating with a biotinylated secondary antibody at a concentration of 1:1000 (BA-1000-1.5, Palex) in 1X TBS with 2% NGS for 1 hour at RT. After rinsing for 5 minutes 3 times with 1X TBS samples were incubated with the Ultra-Sensitive ABC Peroxidase Standard Staining Kit (32050, Thermo Fisher Scientific) for 1 hour. Samples were once again rinsed for 5 minutes 3 times with 1X TBS. Vector SG Peroxidase Substrate Kit (Vector Laboratories) was the chromogen used for 15 minutes to stain the tissue. Samples were rinsed for 5 minutes 3 times. To dehydrate the tissue, samples were sequentially transferred to a 70% ethanol solution for 2 minutes, a 95% ethanol solution for 2 minutes, a 100% ethanol solution for 2 minutes and 2 times to a xylene solution for 5 minutes. Finally, the slides were coverslipped using the DPX mounting medium (Sigma-Aldrich).

For Image acquisition and cell quantification, brain slides were scanned at 20x high resolution using an Olympus Slideview VS200 slide scanner. Scanned sections were then analyzed with a specifically trained A-powered algorithm using the Olympus V200 Desktop 3.3 software to quantify IBA-1+ cells and their morphology (i.e. ramified, amoeboid) as previously reported[20]. All countings were manually revised by an investigator blind to the experimental groups.

Data analysis and statistics

Statistical analyses were performed using GraphPad PRISM 7 (GraphPad Software Inc.). Results are presented as Mean ± Standard Error to the Mean (SEM) of three biological independent experiments. Normal distribution of the samples was assessed by the Shapiro-Wilk test to determine the use of parametric or non-parametric tests. Outlier values were measured with the Grubbs' test by setting an α of 0.05. Statistical comparisons between two groups were evaluated by using Two-tailed unpaired Student's T-test for parametric comparisons. For more than two groups, ordinary One- or Two-way Analysis of Variance (ANOVA) test was used followed by Tukey's multiple comparison test. Values of $p<0.05$ were considered statistically significant.

Data availability

The authors declare that data suporting the findings of this study are available within the paper and its supplementary information files.

References

1. Dickson, D. W. Neuropathology of Parkinson disease. *Parkinsonism Relat. Disord.* **46 Suppl 1**, S30–S33 (2018).
2. Tansey, M. G. *et al.* Inflammation and immune dysfunction in Parkinson disease. *Nat. Rev. Immunol.* **22**, 657–673 (2022).
3. Pang, S. Y.-Y. *et al.* The interplay of aging, genetics and environmental factors in the pathogenesis of Parkinson's disease. *Transl. Neurodegener.* **8**, 23 (2019).
4. Skrahina, V. *et al.* The Rostock International Parkinson's Disease (ROPAD) Study: Protocol and Initial Findings. *Mov. Disord. Off. J. Mov. Disord. Soc.* **36**, 1005–1010 (2021).
5. Di Maio, R. *et al.* LRRK2 activation in idiopathic Parkinson's disease. *Sci. Transl. Med.* **10**, eaar5429 (2018).
6. Wallings, R., Manzoni, C. & Bandopadhyay, R. Cellular processes associated with LRRK2 function and dysfunction. *FEBS J.* **282**, 2806–2826 (2015).
7. Gardet, A. *et al.* LRRK2 is involved in the IFN-gamma response and host response to pathogens. *J. Immunol. Baltim. Md 1950* **185**, 5577–5585 (2010).
8. Hakimi, M. *et al.* Parkinson's disease-linked LRRK2 is expressed in circulating and tissue immune cells and upregulated following recognition of microbial structures. *J. Neural Transm.* **118**, 795–808 (2011).
9. Cook, D. A. *et al.* LRRK2 levels in immune cells are increased in Parkinson's disease. *Npj Park. Dis.* **3**, 11 (2017).
10. Kozina, E. *et al.* Mutant LRRK2 mediates peripheral and central immune responses leading to neurodegeneration in vivo. *Brain* **141**, 1753–1769 (2018).
11. Moehle, M. S. *et al.* LRRK2 Inhibition Attenuates Microglial Inflammatory Responses. *J. Neurosci.* **32**, 1602–1611 (2012).

12. Gillardon, F., Schmid, R. & Draheim, H. Parkinson's disease-linked leucine-rich repeat kinase 2(R1441G) mutation increases proinflammatory cytokine release from activated primary microglial cells and resultant neurotoxicity. *Neuroscience* **208**, 41–48 (2012).
13. Marker, D. F. *et al.* LRRK2 kinase inhibition prevents pathological microglial phagocytosis in response to HIV-1 Tat protein. *J. Neuroinflammation* **9**, 752 (2012).
14. Lee, H. *et al.* LRRK2 Is Recruited to Phagosomes and Co-recruits RAB8 and RAB10 in Human Pluripotent Stem Cell-Derived Macrophages. *Stem Cell Rep.* **14**, 940–955 (2020).
15. Panagiotakopoulou, V. *et al.* Interferon-γ signaling synergizes with LRRK2 in neurons and microglia derived from human induced pluripotent stem cells. *Nat. Commun.* **11**, 5163 (2020).
16. Hirsch, E. C., Graybiel, A. M. & Agid, Y. Selective vulnerability of pigmented dopaminergic neurons in Parkinson's disease. *Acta Neurol. Scand. Suppl.* **126**, 19–22 (1989).
17. Kastner, A. *et al.* Is the vulnerability of neurons in the substantia nigra of patients with Parkinson's disease related to their neuromelanin content? *J. Neurochem.* **59**, 1080–1089 (1992).
18. Zucca, F. A. *et al.* Neuromelanin of the human substantia nigra: an update. *Neurotox. Res.* **25**, 13–23 (2014).
19. Carballo-Carbajal, I. *et al.* Brain tyrosinase overexpression implicates age-dependent neuromelanin production in Parkinson's disease pathogenesis. *Nat. Commun.* **10**, 973 (2019).

20. Gonzalez-Sepulveda, M. *et al.* In vivo reduction of age-dependent neuromelanin accumulation mitigates features of Parkinson's disease. *Brain* **146**, 1040–1052 (2023).
21. Chocarro, J. *et al.* Neuromelanin accumulation drives endogenous synucleinopathy in non-human primates. *Brain* **146**, 5000–5014 (2023).
22. Wilms, H. *et al.* Activation of microglia by human neuromelanin is NF-kappaB dependent and involves p38 mitogen-activated protein kinase: implications for Parkinson's disease. *FASEB J. Off. Publ. Fed. Am. Soc. Exp. Biol.* **17**, 500–502 (2003).
23. Vila, M. Neuromelanin, aging, and neuronal vulnerability in Parkinson's disease. *Mov. Disord. Off. J. Mov. Disord. Soc.* **34**, 1440–1451 (2019).
24. Zecca, L. *et al.* Human neuromelanin induces neuroinflammation and neurodegeneration in the rat substantia nigra: implications for Parkinson's disease. *Acta Neuropathol. (Berl.)* **116**, 47–55 (2008).
25. Ferrari, E. *et al.* Synthesis, Structure Characterization, and Evaluation in Microglia Cultures of Neuromelanin Analogues Suitable for Modeling Parkinson's Disease. *ACS Chem. Neurosci.* **8**, 501–512 (2017).
26. Galiano-Landeira, J., Torra, A., Vila, M. & Bové, J. CD8 T cell nigral infiltration precedes synucleinopathy in early stages of Parkinson's disease. *Brain* **143**, 3717–3733 (2020).
27. Zhang, W. *et al.* Neuromelanin activates microglia and induces degeneration of dopaminergic neurons: implications for progression of Parkinson's disease. *Neurotox. Res.* **19**, 63–72 (2011).
28. Tejchman-Skrzyszewska, A. *et al. Synthetic Neuromelanin as a Trigger of Inflammation in the Brain – New Mouse Model of Parkinson's Disease*.

http://biorxiv.org/lookup/doi/10.1101/2023.04.28.538536 (2023) doi:10.1101/2023.04.28.538536.

29. Douvaras, P. *et al.* Directed Differentiation of Human Pluripotent Stem Cells to Microglia. *Stem Cell Rep.* **8**, 1516–1524 (2017).
30. Mesci, P. *et al.* Modeling neuro-immune interactions during Zika virus infection. *Hum. Mol. Genet.* **27**, 41–52 (2018).
31. Butovsky, O. *et al.* Identification of a unique TGF-β–dependent molecular and functional signature in microglia. *Nat. Neurosci.* **17**, 131–143 (2014).
32. Parnetti, L. *et al.* Cerebrospinal fluid biomarkers in Parkinson disease. *Nat. Rev. Neurol.* **9**, 131–140 (2013).
33. Williams-Gray, C. H. *et al.* Serum immune markers and disease progression in an incident Parkinson's disease cohort (ICICLE-PD). *Mov. Disord. Off. J. Mov. Disord. Soc.* **31**, 995–1003 (2016).
34. Nagatsu, T., Mogi, M., Ichinose, H. & Togari, A. Changes in cytokines and neurotrophins in Parkinson's disease. *J. Neural Transm. Suppl.* 277–290 (2000) doi:10.1007/978-3-7091-6301-6_19.
35. Hofmann, K. W. *et al.* Interleukin-6 serum levels in patients with Parkinson's disease. *Neurochem. Res.* **34**, 1401–1404 (2009).
36. Scalzo, P., Kümmer, A., Cardoso, F. & Teixeira, A. L. Increased serum levels of soluble tumor necrosis factor-alpha receptor-1 in patients with Parkinson's disease. *J. Neuroimmunol.* **216**, 122–125 (2009).
37. Qin, X.-Y., Zhang, S.-P., Cao, C., Loh, Y. P. & Cheng, Y. Aberrations in Peripheral Inflammatory Cytokine Levels in Parkinson Disease: A Systematic Review and Meta-analysis. *JAMA Neurol.* **73**, 1316–1324 (2016).

38. Aguzzi, A., Barres, B. A. & Bennett, M. L. Microglia: scapegoat, saboteur, or something else? *Science* **339**, 156–161 (2013).

39. Paolicelli, R. C. *et al.* Synaptic pruning by microglia is necessary for normal brain development. *Science* **333**, 1456–1458 (2011).

40. Stephan, A. H., Barres, B. A. & Stevens, B. The complement system: an unexpected role in synaptic pruning during development and disease. *Annu. Rev. Neurosci.* **35**, 369–389 (2012).

41. Gerhard, A. *et al.* In vivo imaging of microglial activation with [11C](R)-PK11195 PET in idiopathic Parkinson's disease. *Neurobiol. Dis.* **21**, 404–412 (2006).

42. Stokholm, M. G. *et al.* Assessment of neuroinflammation in patients with idiopathic rapid-eye-movement sleep behaviour disorder: a case-control study. *Lancet Neurol.* **16**, 789–796 (2017).

43. Bartels, A. L. *et al.* [11C]-PK11195 PET: quantification of neuroinflammation and a monitor of anti-inflammatory treatment in Parkinson's disease? *Parkinsonism Relat. Disord.* **16**, 57–59 (2010).

44. Gonzalez-Sepulveda, M. *et al.* Validation of a Reversed Phase UPLC-MS/MS Method to Determine Dopamine Metabolites and Oxidation Intermediates in Neuronal Differentiated SH-SY5Y Cells and Brain Tissue. *ACS Chem. Neurosci.* **11**, 2679–2687 (2020).

45. di Domenico, A. *et al.* Patient-Specific iPSC-Derived Astrocytes Contribute to Non-Cell-Autonomous Neurodegeneration in Parkinson's Disease. *Stem Cell Rep.* **12**, 213–229 (2019).

46. Xie, Y., Jin, C., Sang, H., Liu, W. & Wang, J. Ivermectin Protects Against Experimental Autoimmune Encephalomyelitis in Mice by Modulating the

Th17/Treg Balance Involved in the IL-2/STAT5 Pathway. *Inflammation* **46**, 1626–1638 (2023).

47. Zabala, A. *et al.* P2X4 receptor controls microglia activation and favors remyelination in autoimmune encephalitis. *EMBO Mol. Med.* **10**, e8743 (2018).
48. Liddelow, S. A. *et al.* Neurotoxic reactive astrocytes are induced by activated microglia. *Nature* **541**, 481–487 (2017).
49. Kempuraj, D. *et al.* Neuroinflammation Induces Neurodegeneration. *J. Neurol. Neurosurg. Spine* **1**, 1003 (2016).
50. Booth, H. D. E., Hirst, W. D. & Wade-Martins, R. The Role of Astrocyte Dysfunction in Parkinson's Disease Pathogenesis. *Trends Neurosci.* **40**, 358–370 (2017).
51. Nagatsu, T., Nakashima, A., Watanabe, H., Ito, S. & Wakamatsu, K. Neuromelanin in Parkinson's Disease: Tyrosine Hydroxylase and Tyrosinase. *Int. J. Mol. Sci.* **23**, 4176 (2022).
52. Laguna, A. *et al. Modelling Human Brain-Wide Pigmentation in Rodents Recapitulates Age-Related Multisystem Neurodegenerative Deficits*. http://biorxiv.org/lookup/doi/10.1101/2023.08.08.552400 (2023) doi:10.1101/2023.08.08.552400. Accepted in *Nature Communication*
53. Butovsky, O. & Weiner, H. L. Microglial signatures and their role in health and disease. *Nat. Rev. Neurosci.* **19**, 622–635 (2018).
54. Speidel, A., Felk, S., Reinhardt, P., Sterneckert, J. & Gillardon, F. Leucine-Rich Repeat Kinase 2 Influences Fate Decision of Human Monocytes Differentiated from Induced Pluripotent Stem Cells. *PloS One* **11**, e0165949 (2016).
55. Choi, I. *et al.* LRRK2 G2019S mutation attenuates microglial motility by inhibiting focal adhesion kinase. *Nat. Commun.* **6**, 8255 (2015).

56. Ohtonen, S. *et al.* Human iPSC-derived microglia carrying the LRRK2-G2019S mutation show a Parkinson's disease related transcriptional profile and function. *Sci. Rep.* **13**, 22118 (2023).

57. Ho, D. H., Seol, W., Eun, J. H. & Son, I. Phosphorylation of p53 by LRRK2 induces microglial tumor necrosis factor α-mediated neurotoxicity. *Biochem. Biophys. Res. Commun.* **482**, 1088–1094 (2017).

58. Ho, D. H. *et al.* LRRK2 Kinase Activity Induces Mitochondrial Fission in Microglia via Drp1 and Modulates Neuroinflammation. *Exp. Neurobiol.* **27**, 171–180 (2018).

59. Orr, C. F., Rowe, D. B., Mizuno, Y., Mori, H. & Halliday, G. M. A possible role for humoral immunity in the pathogenesis of Parkinson's disease. *Brain* **128**, 2665–2674 (2005).

60. Beach, T. G. *et al.* Marked microglial reaction in normal aging human substantia nigra: correlation with extraneuronal neuromelanin pigment deposits. *Acta Neuropathol. (Berl.)* **114**, 419–424 (2007).

61. Depboylu, C. *et al.* Possible Involvement of Complement Factor C1q in the Clearance of Extracellular Neuromelanin From the Substantia Nigra in Parkinson Disease. *J. Neuropathol. Exp. Neurol.* **70**, 125–132 (2011).

62. Walker, D., Lue, L.-F., Beach, T. & Tooyama, I. Microglial Phenotyping in Neurodegenerative Disease Brains: Identification of Reactive Microglia with an Antibody to Variant of CD105/Endoglin. *Cells* **8**, 766 (2019).

63. Yanagimachi, M. D. *et al.* Robust and Highly-Efficient Differentiation of Functional Monocytic Cells from Human Pluripotent Stem Cells under Serum- and Feeder Cell-Free Conditions. *PLoS ONE* **8**, e59243 (2013).

64. Kriks, S. *et al.* Dopamine neurons derived from human ES cells efficiently engraft in animal models of Parkinson's disease. *Nature* **480**, 547–551 (2011).

65. Fedele, S. *et al.* Expansion of human midbrain floor plate progenitors from induced pluripotent stem cells increases dopaminergic neuron differentiation potential. *Sci. Rep.* **7**, 6036 (2017).

66. Chambers, S. M. *et al.* Highly efficient neural conversion of human ES and iPS cells by dual inhibition of SMAD signaling. *Nat. Biotechnol.* **27**, 275–280 (2009).

67. Sánchez-Danés, A. *et al.* Efficient Generation of A9 Midbrain Dopaminergic Neurons by Lentiviral Delivery of LMX1A in Human Embryonic Stem Cells and Induced Pluripotent Stem Cells. *Hum. Gene Ther.* **23**, 56–69 (2012).

68. Haenseler, W. *et al.* A Highly Efficient Human Pluripotent Stem Cell Microglia Model Displays a Neuronal-Co-culture-Specific Expression Profile and Inflammatory Response. *Stem Cell Rep.* **8**, 1727–1742 (2017).

69. Ferreira, T. A. *et al.* Neuronal morphometry directly from bitmap images. *Nat. Methods* **11**, 982–984 (2014).

70. Tristán-Noguero, A. *et al.* iPSC -based modeling of THD recapitulates disease phenotypes and reveals neuronal malformation. *EMBO Mol. Med.* **15**, e15847 (2023).

71. Byun, Y. G. & Chung, W.-S. A Novel In Vitro Live-imaging Assay of Astrocyte-mediated Phagocytosis Using pH Indicator-conjugated Synaptosomes. *J. Vis. Exp.* 56647 (2018) doi:10.3791/56647.

72. Sellgren, C. M. *et al.* Patient-specific models of microglia-mediated engulfment of synapses and neural progenitors. *Mol. Psychiatry* **22**, 170–177 (2017).

73. d'Ischia, M. *et al.* Melanins and melanogenesis: methods, standards, protocols. *Pigment Cell Melanoma Res.* **26**, 616–633 (2013).

Acknowledgments

The authors are indebted to the patients with PD who have participated in this study; the Neurological Tissue Bank of the Biobank-Hospital Clinic-IDIBAPS (Barcelona, Spain) for human sample procurement. The authors thank Giulia Carola for helping with some culture experiments. Research from the authors' laboratories is supported by the Spanish Ministry of Science and Innovation-MICINN (PID2020-116339RB-I00, PID2021-123925OB-I00, and PID2022-139546OB-I00 supported by MCIN/AEI/10.13039/501100011033 and FEDER, and PDC2021-121051-I00 supported by MCIN/AEI/10.13039/501100011033 and by the European Union Next Generation EU/ PRTR); Instituto de Salud Carlos III-ISCIII/FEDER (Red de Terapia Celular- TerCel RD16/0011/0024); AGAUR (2021-SGR-974), the Marató de TV3 Foundation (202012-32 and 202331-30); CERCA Program / Generalitat de Catalunya; Aligning Science Across Parkinson's through The Michael J. Fox Foundation for Parkinson's Research, USA (ASAP-020505 to MV); La Caixa Bank Foundation, Spain (Health Research Grant, ID 100010434 under the agreement LCF/PR/HR17/52150003 to MV). LB was the recipient of a pre-doctoral fellowship FPI (BES-2017-080579) from the Spanish Ministry of Economy and Competitiveness (MINECO). VT and JC were received a pre-doctoral La Caixa INPhINIT Incoming Fellowship (code: LCF/BQ/DI21/11860038 for VT and code: LCF/BQ/DI18/1166063 for JC). VB was the recipient of a pre-doctoral fellowship FPI (PRE2020-094465) from the Spanish Ministry of Economy and Competitiveness (MINECO). AC is a recipient of an ICREA "Academia" Award (Generalitat de Catalunya).

Author contributions

Conceptualization, A.C., M.V., A.R.; Methodology & Formal Analysis, L.B., M.P.,V.T., G.R., J.M., I.F.,Y.R-P., M.G-S., T.C., J.M.C-S, J.C.; Writing-Original Draft, M.P., V.T., A.C., M.V., A.R.; Writing-Review & Editing, all authors.

Competing interests

The Authors declare no competing financial interests.

Figure Legends

Figure 1. Characterization of hMG cells. a Representative ICC images of iPSC-derived hMG after 7 days in culture from CTL (SP09), L2-PD (L2-PD1: SP12) and L2-PD^{corr} (L2-PD1^{corr}: SP12wt/wt) iPSC lines staining positive for IBA-1, CX3CR1 or TMEM-119 (green) and negative for astrocytic (GFAP) or neuronal (TUJ1) markers. Scale bar=50 µm. Nuclei are counterstained with DAPI (blue). **b** Percentage of hMG cells expressing IBA-1, CX3CR1 or TMEM-119 in respect to DAPI. **c** Schematic representation of LPS stimulation (100ng/ml). **d-f** Cytokine profile for IL-1β (**d**), IL-6 (**e**) and TNF-α (**f**) of all hMG under basal condition and after 24 hours of LPS stimulation. **g** Representative Bright Field and Red fluorescent images of CTL (SP09), L2-PD1 (SP12), L2-PD2 (SP13), L2-PD1^{corr} (SP12wt/wt) and L2-PD2^{corr} (SP13wt/wt) hMG phagocyting pHrodo labelled SYNs after 150min of exposure to SYNs (time scale=hours; scale bar=25 µm). **h** Area Under the Curve (AUC) of Phagocytic Index (PI) representing red fluorescent intensity of phagocyted SYNs by hMG over 5 hours. N=3 independent experiments for every line. Bars and error bars represent Mean ± SEM. Two-way ANOVA with Tukey's multiple comparison test; *p<0.05, **p<0.01, ***p<0.001.

Figure 2. L2-PD hMG Increase Neuromelanin particle phagocytosis and induce the expression of pro-inflammatory cytokines and ROS. a Schematic representation of NM stimulation (5ug/ml) and following analyses. **b** Representative Bright Field images of L2-PD (L2-PD1: SP12; L2-PD2: SP13), and L2-PD^{corr} (L2-PD1^{corr}: SP12wt/wt; L2-PD2^{corr} SP13wt/wt) hMG phagocyting NM particles for 16 hours (yellow arrow-heads for phagocyted particles; time scale=hours; scale bar=25 µm). **c** AUC of NM particle uptake per hMG cell over 16 hours. **d.** Spontaneous migration paths of L2-PD (L2-PD1: SP12; L2-PD2: SP13), and L2-PD^{corr} (L2-PD1^{corr}: SP12wt/wt; L2-PD2^{corr} SP13wt/wt) hMG (around 15 cells each) were tracked for 16h. The location of each cell was determined every 2 minutes and connected to depict its migration route. **e-f** Quantification of velocity (**e**; µm/minute) and Euclidean distances (**f**; µm). **g-j** Relative mRNA expression of pro-inflammatory cytokines TNF-α (**g**), IL-1β (**h**), C3 (**i**), and IL-6 (**j**) in L2-PD (L2-PD1: SP12; L2-PD2: SP13), and L2-PD^{corr} (L2-PD1^{corr}: SP12wt/wt; L2-PD2^{corr} SP13wt/wt) hMG at basal conditions or under NM stimulation for 24 hours. **k** Intracellular ROS by DCFH-DA intensity after NM stimulation in L2-PD (L2-PD1: SP12; L2-PD2: SP13), and L2-PD^{corr} (L2-PD1^{corr}: SP12wt/wt; L2-PD2^{corr} SP13wt/wt) hMG. Results are represented as a fold change between NM stimulation for 24 hours over non-stimulated conditions. Student t-test or Mann-Whitney test for non-parametric conditions were when only two groups were compared. N=3-4 independent experiments for every line. Bars and error bars

represent Mean ± SEM. One-Way ANOVA with Tukey's multiple comparison test; $p<0.05$, $^{**}p<0.01$, $^{***}p<0.001$.

Figure 3. L2-PD hMG exposed to NM induce dopaminergic degeneration in an iPSC-derived 2D neuron/hMG co-culture system. a Schematic representation of the co-culture system and neuromelanin (NM) or Ivermectin (IVM) stimulation. Briefly, CTL (SP11) DAn were plated on top of astrocytes feeder layer on Day 0. One week later, L2-PD (SP13) or L2-PD^{corr} (SP13wt/wt) hMG were plated on top of DAn and exposed to NM at Day 14 for 8 hours, with or without treatment with IVM for 6 hours. **b-c** Representative ICC images of L2-PD2^{corr} (SP13wt/wt) (**b**) or L2-PD2 (SP13) (**c**) IBA1 + hMG (Red) in culture with TH+ DAn (Green) under basal conditions. In white TUJ1 + neurons (Scale bar=25 µm). **d** Representative images of TH+ DAn upon culture with L2-PD2^{corr} hMG (SP13wt/wt), without or with NM (Scale bar=25 µm**)**. **e** Quantification of percentage of TH+ population over the total number of DAPI+ cells (normalized over L2-PD^{corr} percentage) in L2-PD^{corr} hMG. **f** Representative images of TH+ DAn upon culture with L2-PD2 hMG (SP13), without or with NM (Scale bar=25 µm**). g** Quantification of percentage of TH+ population over the total number of DAPI+ cells (normalized over L2-PD^{corr} percentage) in L2-PD hMG. **h** Representative images of DAn (TH+) cultured with L2-PD hMG (L2-PD2: SP13) upon addition of NM or treatment with IVM and NM (Scale bar=25 µm**). i** Quantification of percentage of TH+ population over the number of DAPI+ cells without or with IVM treatment (normalized over NM only addition percentage). **j-m** Relative mRNA expression of pro-inflammatory cytokines *IL*-6 (**j**), IL-*1β* (**k**), *TNFα* (**l**) and *C3* (**m**) in L2-PD hMG treated with NM and IVM. Student t-test or Mann-Whitney test for non-parametric conditions were when only two groups were compared. N=3 independent experiments for every line. Bars and error bars represent Mean ± SEM. One-Way ANOVA with Tukey's multiple comparison test; $p<0.05$, $^{**}p<0.01$, $^{***}p<0.001$.

Figure 4. Microglial activation is increased in L2-PD patient post-mortem brains. **a** Total number of IBA-1+ cells/mm^2 in post-mortem human brains from control subjects and L2-PD patients. **b** Number of IBA-1+ cells displaying ramified and amoeboid morphologies in control and L2-PD brains. **c** Representative images of IBA-1+ cells (in blue; unstained NM in brown) from control and L2-PD human brains showing ramified (white arrowhead) or amoeboid (black arrowhead) morphologies. Grey arrowheads indicate NM-laden neurons. N=32 Control subjects and N=6 L2-PD patients. Bars represent Mean ± SEM. In **a**, * $p<0.05$ versus Control (Mann-Whitney test). In **b**, $^{***}p<0.001$ versus corresponding (amoeboid) Control (Two-way ANOVA; Sidak multiple comparison test within morphology groups).

Table 1. Summary of the healthy controls and patients used in this study

Cell line code	Status	Code used in this study	Sex	Age at donation	Age at onset	LRRK2 mutation	Isogenic control
SP-11	Control	CTL	F	48	-	No	-
SP-09	Control	CTL	M	66	-	No	-
SP-12	L2-PD	L2-PD1	F	63	49	G2019S	-
SP-13	L2-PD	L2-PD2	F	68	57	G2019S	-
SP-12 wt/wt	Isogenic Control	L2-PD1^{corr}	F	63	-	G2019S	LRRK2^{G2019S} corrected
SP-13 wt/wt	Isogenic Control	L2-PD2^{corr}	F	68	-	G2019S	LRRK2^{G2019S} corrected

Table 2. Human Sample information

Case	Gender	Age at death (years)	Disease duration (years)	PMI (hr)	Braak PD staging
Control-1	Female	59	-	2	-
Control-2	Male	59	-	6	-
Control-3	Male	59	-	5	-
Control-4	Male	60	-	N/A	-
Control-5	Female	60	-	N/A	-
Control-6	Female	61	-	N/A	-
Control-7	Female	62	-	2	-
Control-8	Male	63	-	N/A	-
Control-9	Male	63	-	12	-
Control-10	Female	65	-	N/A	-
Control-11	Male	65	-	N/A	-
Control-12	Female	66	-	N/A	-
Control-13	Male	69	-	N/A	-
Control-14	Female	70	-	14	-
Control-15	Female	70	-	N/A	-
Control-16	Female	71	-	N/A	-
Control-17	Female	73	-	N/A	-
Control-18	Female	74	-	N/A	-
Control-19	Male	76	-	11.5	-
Control-20	Male	78	-	4	-
Control-21	Female	79	-	N/A	-

Control-22	Female	79	-	N/A	-
Control-23	Male	81	-	2	-
Control-24	Male	83	-	13	-
Control-25	Female	83	-	7.2	-
Control-26	Female	83	-	4	-
Control-27	Male	84	-	4	-
Control-28	Female	86	-	4	-
Control-29	Female	90	-	12.25	-
Control-30	Female	91	-	8	-
Control-31	Male	91	-	N/A	-
Control-32	Female	94	-	N/A	-
L2-PD-1	Male	84	N/A	20	I-II
L2-PD-2	Female	78	26	27.5	IV
L2-PD-3	Female	77	10	8	N/A
L2-PD-4	Female	93	15	7	IV
L2-PD-5	Female	69	17	12.5	V
L2-PD-6	Male	69	N/A	15.5	N/A

L2-PD: LRRK2-PD; PMI: post-mortem interval (hours); N/A: Not available.

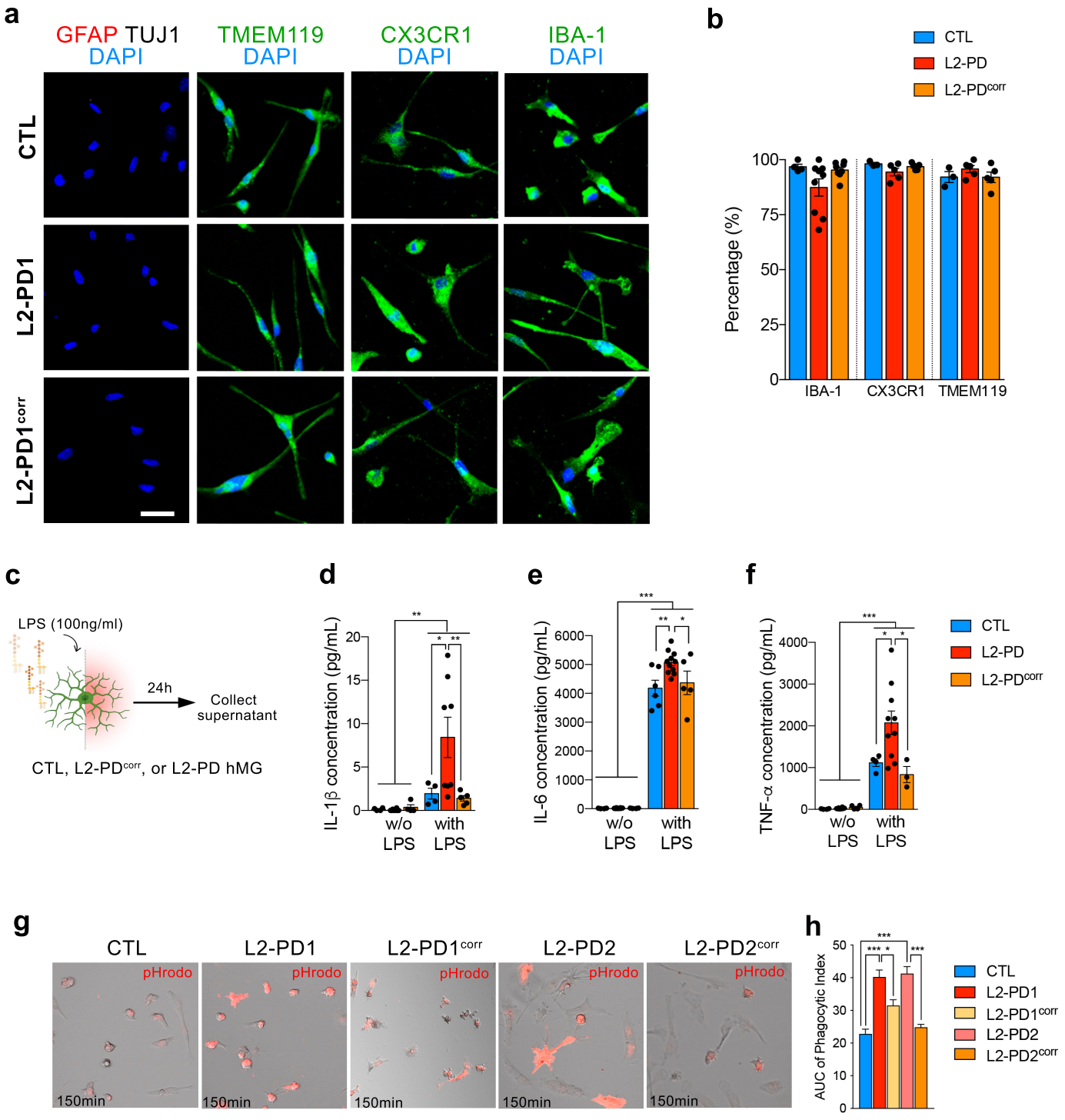
a
GFAP TUJ1 DAPI
TMEM119 DAPI
CX3CR1 DAPI
IBA-1 DAPI
CTL
L2-PD1
L2-PD1corr
b
CTL
L2-PD
L2-PDcorr
Percentage (%)
IBA-1
CX3CR1
TMEM119
c
LPS (100ng/ml)
24h
Collect supernatant
CTL, L2-PDcorr, or L2-PD hMG
d
IL-1β concentration (pg/mL)
w/o LPS
with LPS
e
IL-6 concentration (pg/mL)
f
TNF-α concentration (pg/mL)
g
CTL
L2-PD1
L2-PD1corr
L2-PD2
L2-PD2corr
pHrodo
150min
h
AUC of Phagocytic Index

FIGURE 1

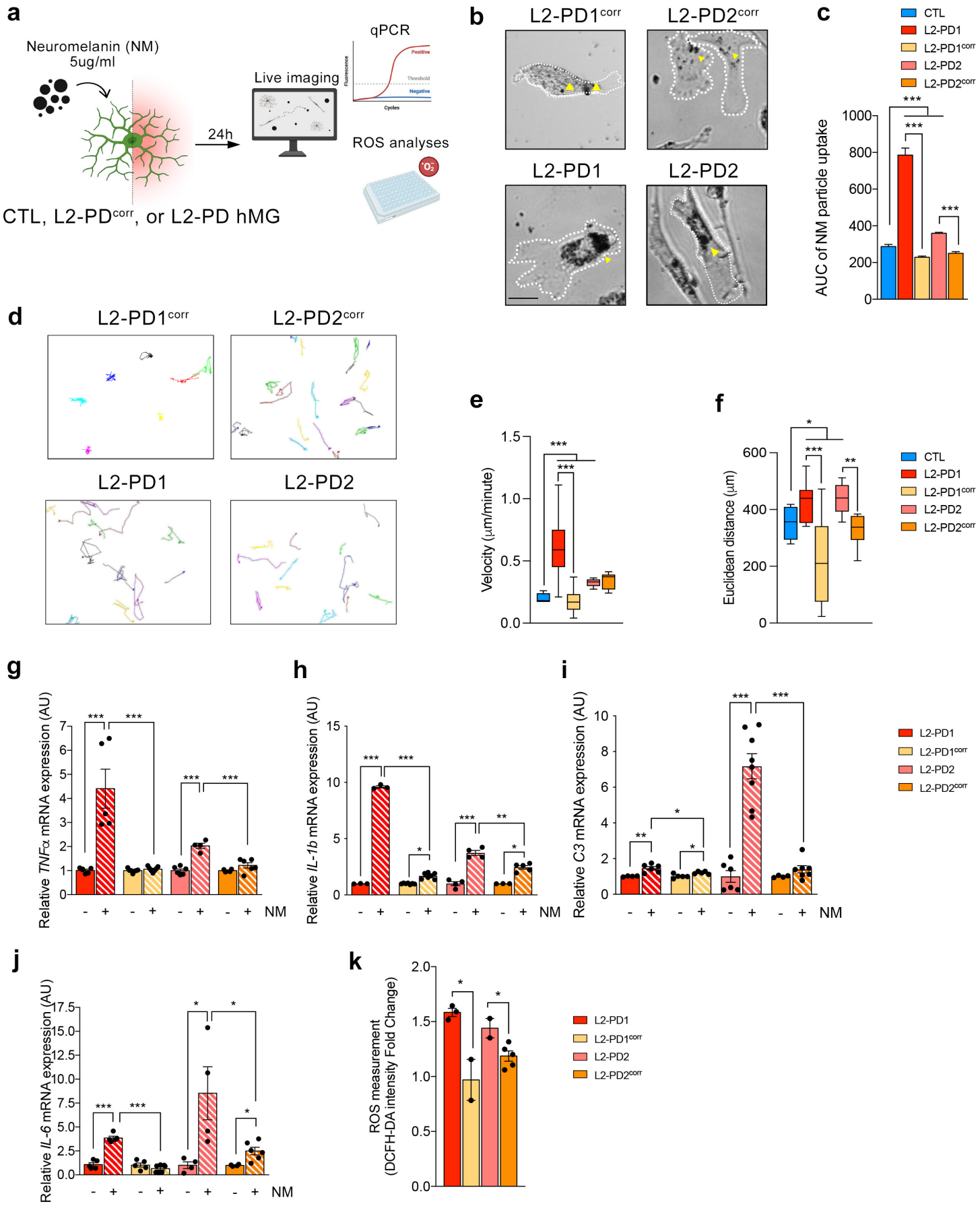
a
Neuromelanin (NM)
5ug/ml
24h
Live imaging
qPCR
Positive
Threshold
Negative
Fluorescence
Cycles
ROS analyses
CTL, L2-PDcorr, or L2-PD hMG
b
L2-PD1corr
L2-PD2corr
L2-PD1
L2-PD2
c
CTL
L2-PD1
L2-PD1corr
L2-PD2
L2-PD2corr
AUC of NM particle uptake
d
L2-PD1corr
L2-PD2corr
L2-PD1
L2-PD2
e
Velocity (µm/minute)
f
Euclidean distance (µm)
g
Relative TNFα mRNA expression (AU)
h
Relative IL-1b mRNA expression (AU)
i
Relative C3 mRNA expression (AU)
NM
j
Relative IL-6 mRNA expression (AU)
k
ROS measurement
(DCFH-DA intensity Fold Change)

FIGURE 2

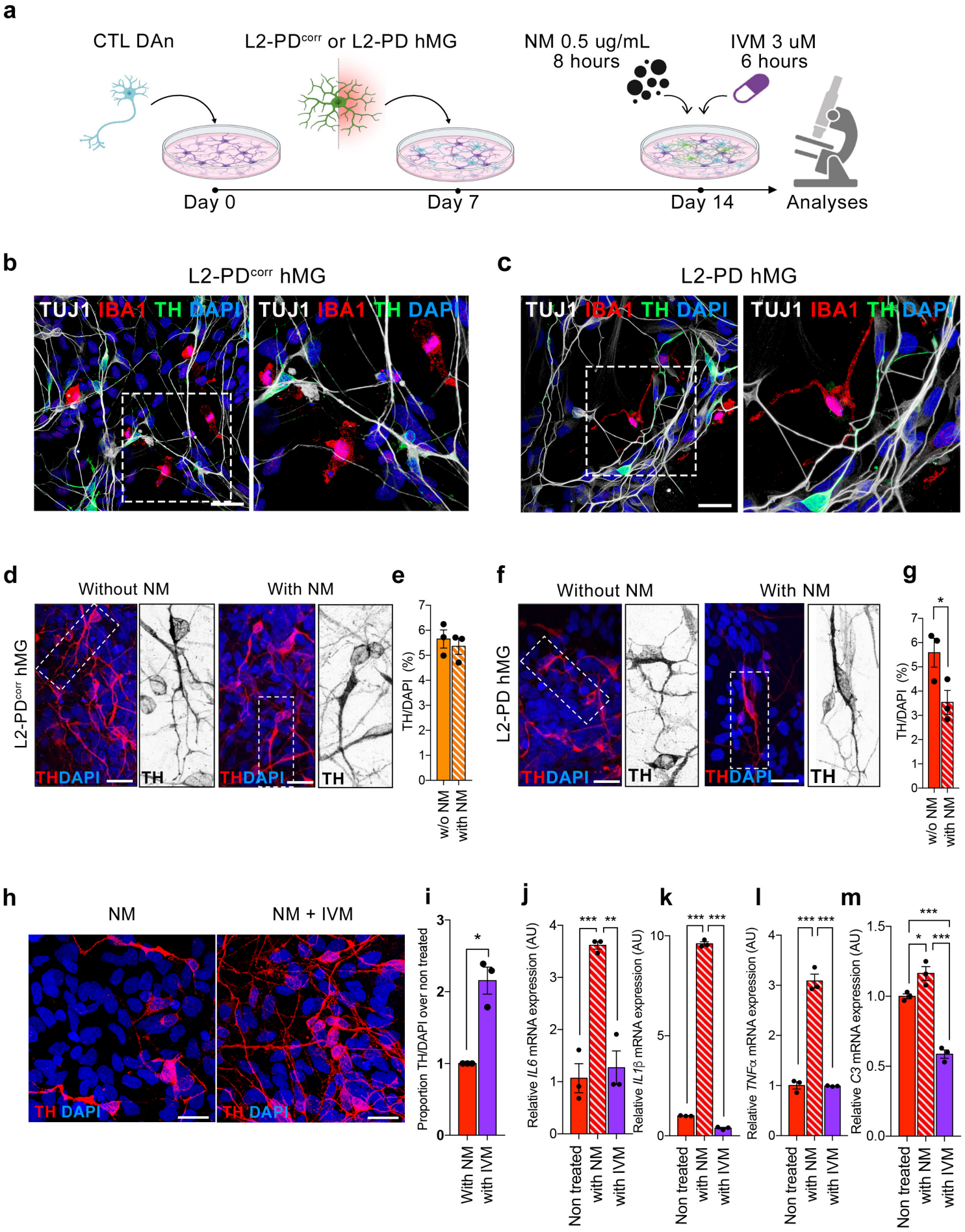
a
CTL DAn
L2-PDcorr or L2-PD hMG
NM 0.5 ug/mL
8 hours
IVM 3 uM
6 hours
Day 0
Day 7
Day 14
Analyses
b
L2-PDcorr hMG
TUJ1 IBA1 TH DAPI
c
L2-PD hMG
d
Without NM
With NM
L2-PDcorr hMG
THDAPI
TH
e
TH/DAPI (%)
w/o NM
with NM
f
L2-PD hMG
g
h
NM
NM + IVM
TH DAPI
i
Proportion TH/DAPI over non treated
With NM
with IVM
j
Relative IL6 mRNA expression (AU)
k
Relative IL1β mRNA expression (AU)
l
Relative TNFα mRNA expression (AU)
m
Relative C3 mRNA expression (AU)
Non treated
with NM
with IVM

FIGURE 3

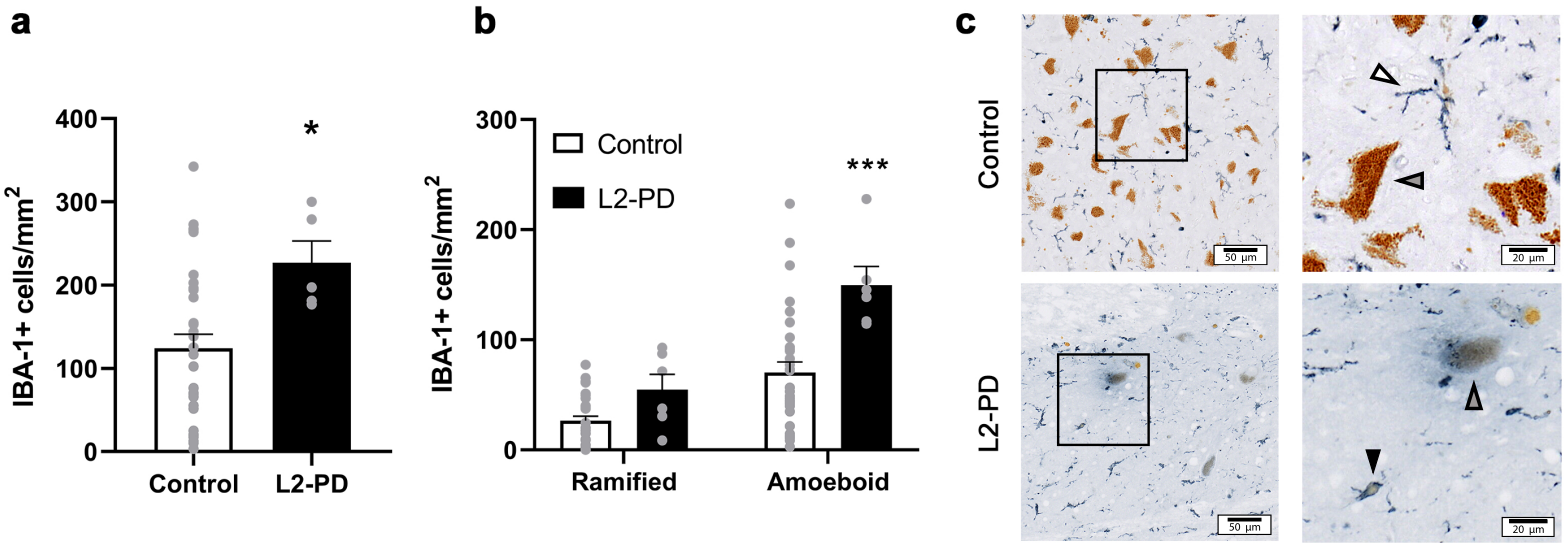
a
400
300
200
100
0
IBA-1+ cells/mm2
*
Control
L2-PD
b
300
200
100
0
IBA-1+ cells/mm2
Control
L2-PD
***
Ramified
Amoeboid
c
Control
L2-PD
50 µm
20 µm
50 µm
20 µm

FIGURE 4